Seismic hazard in southern Calabria (Italy) based on the analysis of a synthetic earthquake catalog

Rodolfo Console, Massimo Chiappini, Liliana Minelli, Fabio Speranza, Roberto Carluccio & Michele Greco

Acta Geophysica

ISSN 1895-6572

Acta Geophys.
DOI 10.1007/s11600-018-0181-7

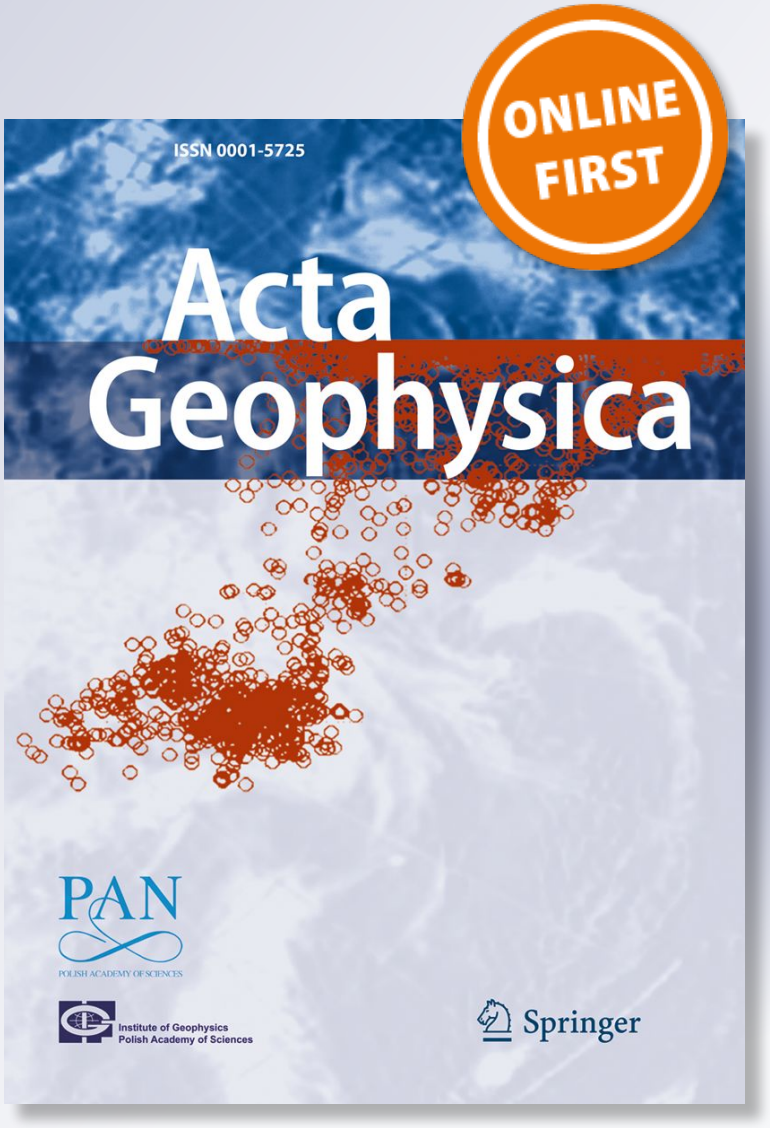

Springer

Acta Geophysica
https://doi.org/10.1007/s11600-018-0181-7

RESEARCH ARTICLE - APPLIED GEOPHYSICS

Seismic hazard in southern Calabria (Italy) based on the analysis of a synthetic earthquake catalog

Rodolfo Console[1,2] · Massimo Chiappini[2] · Liliana Minelli[2] · Fabio Speranza[2] · Roberto Carluccio[2] · Michele Greco[1,3]

Received: 15 January 2018 / Accepted: 17 July 2018

Abstract
The application of a newly developed physics-based earthquake simulator to the active faults inferred by aeromagnetism in southern Calabria has produced a synthetic catalog lasting 100 ky including more than 18,000 earthquakes of magnitude $\geq$ 4.0. This catalog exhibits temporal, spatial and magnitude features, which resemble those of the observed seismicity. As an example of the potential use of synthetic catalogs, a map of the peak ground acceleration (PGA) for a given exceedance probability on the territory under investigation has been produced by means of a simple attenuation law applied to all the events reported in the synthetic catalog. This map was compared with the existing hazard map that is presently used in the national seismic building regulations. The comparison supports a strong similarity of our results with the values given in the present Italian seismic building code, despite the latter being based on a different methodology. The same similarity cannot be recognized for the comparison of our present study with the results obtained from a previous study based on our same methodology but with a different geological model.

Keywords Aeromagnetic survey · Southern Calabria fault system · Fault slip rate · Earthquake simulator · Synthetic earthquake catalog · Probabilistic seismic hazard

Introduction

The Historical Italian Catalog, CPTI15 (Rovida et al. 2015), reports 14 strong events with magnitude ranging from 6.0 to 7.1 since 1600 A.D. in the southern Calabria area, the southernmost portion of the Italian peninsula, close to Sicily, which is one of the regions characterized by the highest seismic hazard in Italy (Fig. 1). This catalog spans a relatively short period, compared with the long inter-event time between characteristic events rupturing single seismogenic faults in this area. In this case, the hypothesis of characteristic event and consequently the estimate of the hazard assessment based on individual seismogenic sources are not supported by observations. In this study, we introduce a multi-methodological approach in order to overcome the problems connected with the uncertainties on the recurrence times of the main earthquake sources. These uncertainties may affect seismic hazard assessment based on statistical models.

Our multi-disciplinary approach is based on the assumption of seismogenic fault geometry and kinematics of southern Calabria as provided by the recent aeromagnetic anomaly data acquisition and interpretation by Minelli et al. (2016). We make use of this seismogenic database through the application of a physics-based earthquake simulator (Console et al. 2015, 2017, 2018), in a way that has become popular in California (Tullis 2012 and references therein, Wilson et al. 2017) and subsequently applied to other seismic regions of the world such as Mexico (Yoder et al. 2015) and New Zealand (Christophersen et al. 2017).

In our simulation algorithm, the seismogenic system is modeled by rectangular fault segments, each of which is discretized in square cells of size set to the minimum

✉ Rodolfo Console
rodolfo.console@ingv.it

[1] Center of Integrated Geomorphology for the Mediterranean Area, CGIAM, Potenza, Italy

[2] Istituto Nazionale di Geofisica e Vulcanologia, INGV, Rome, Italy

[3] University of Basilicata, Potenza, Italy

Published online: 25 July 2018

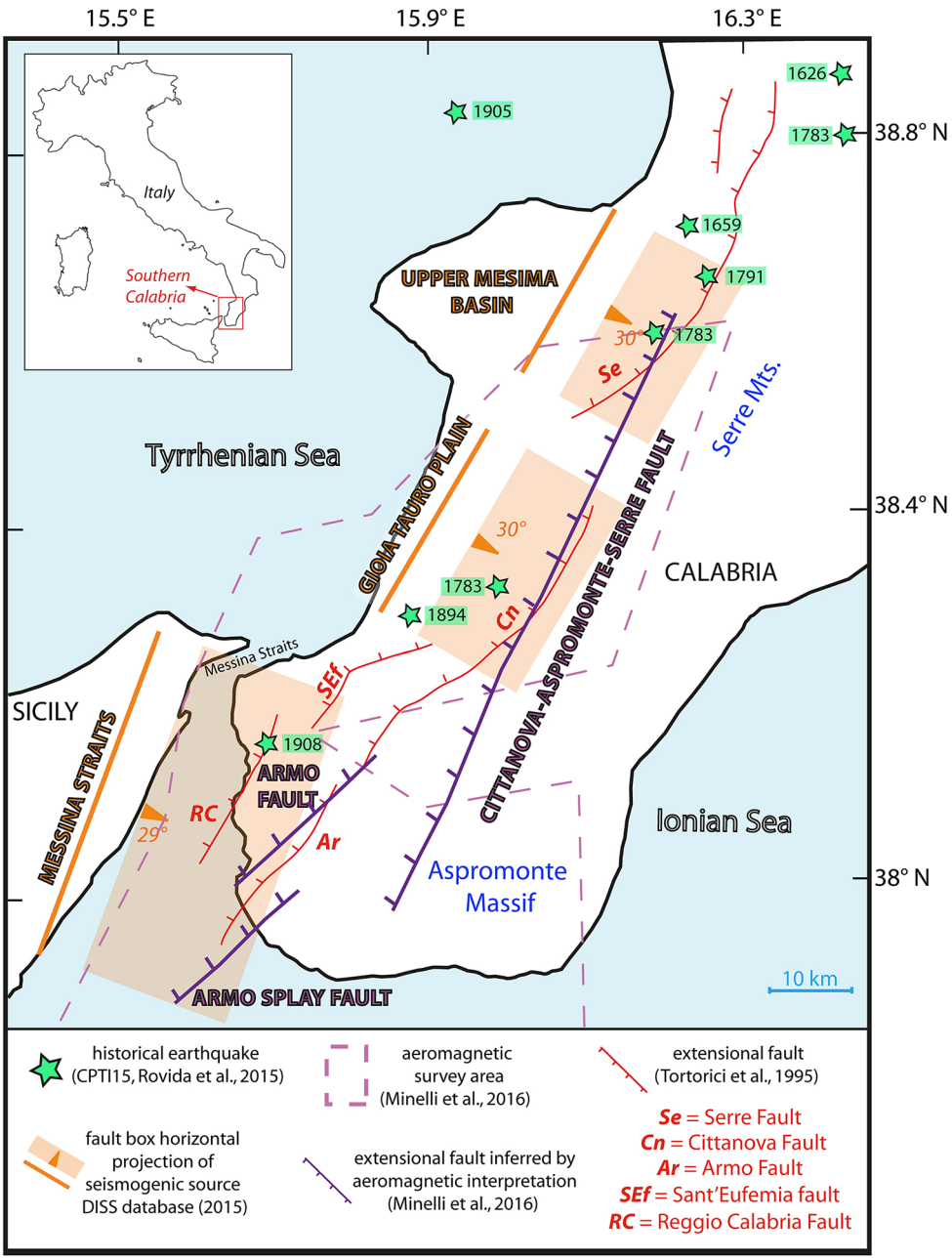

Fig. 1 Synthetic faults map of southern Calabria and northeastern Sicily and epicenters location (denoted by green stars) of the main shocks reported in Table 1. In red, extensional faults proposed by Tortorici et al. (1995), Galli and Bosi (2004) and Aloisi et al. (2013, 2014); in purple, extensional faults inferred by high-resolution aeromagnetic investigation (Minelli et al. 2016); dotted purple line represents the aeromagnetic survey area; in orange, seismogenic sources reported in the DISS database (2015)

earthquake rupture of interest (M = 4.0 in this case). Each cell has an initial stress state that is randomly assigned. Then, each cell is loaded at a steady state proportional to observed slip rates to simulate tectonic stressing. A cell can nucleate an earthquake if its stress value exceeds an assigned strength threshold. After the nucleation occurs, the stress of the ruptured cell is decreased by a static stress drop, and the stress state of all other cells in the model is changed through static stress transfer.

Dynamic rupture propagation is simulated by a reduction of the effective strength in neighboring cells by a value proportional to the square root of the search area, which allows the rupture to expand. The strength reduction is limited if the search area exceeds a given aspect ratio of the rupturing segment, which discourages rupture propagation. A rupture stops when there are no cells with effective strength above the threshold value within the search area. A cell can rupture more than once in the same event.

A rupture can propagate between two defined fault segments if the distance between them is less than a given value (10 km in this application). The simulation algorithm preferentially fills rupture gaps in time and space by nucleating events in cells where the stress budget is higher, which correspond to points where the elapsed time since

Table 1 Major events of the southern Calabria region since 1600 A.D. (from CPTI15)

Year	Month	Day	Latitude	Longitude	Mw
1626	04	04	38.851	16.456	6.03
1659	11	05	38.694	16.249	6.55
1783	02	05	38.297	15.970	7.02
1783	02	07	38.580	16.201	6.62
1783	03	28	38.785	16.464	6.98
1791	10	13	38.636	16.268	6.03
1894	11	16	38.288	15.870	6.07
1905	09	08	38.819	15.943	6.94
1908	12	28	38.146	15.687	7.06

the last rupture is longest. Ruptures also expand toward parts of the faults where the stress budget is highest. Because of the stress transfer included in the model, ruptures tend to initiate close to the termination points of preceding large earthquakes. The earthquake seismic moment is obtained by its definition for each event through the mean event slip and the total ruptured area assuming a shear modulus of $\mu = 30$ GPa. Finally, magnitude is found using the moment–magnitude relation (Hanks and Kanamori 1979).

The third step of our multi-disciplinary approach to seismic hazard assessment is the application of a strong-motion attenuation law to all the events reported in the synthetic catalog for the production of maps showing the peak acceleration (PGA) with a given exceedance probability in a given time period on the territory under investigation.

An approach similar to that outlined above had been already used by Console et al. (2017), but the input structural data were taken from the DISS database (2015) that considers very different seismic sources with respect to Minelli et al. (2016), thus obviously yielding different hazard maps. Our work thus explores the sensitivity of earthquake simulators to seismic source variability for southern Calabria.

Seismotectonics of the Calabrian Arc

The Calabrian Arc represents the emerged portion of a complex accretionary wedge related to the northward subduction of the Ionian oceanic lithosphere beneath the European plate. It extends from the Southern Apennines (to the N) to the northeastern corner of Sicily (to the SW) and is one of the most seismically active areas of the Mediterranean region.

Since the Middle Pleistocene, this region has been affected by ESE-WNW regional extension. In southern Calabria, such extension is accommodated by dip-slip movements along NE–SW striking normal faults (among others Serre, Cittanova, Armo and Reggio Calabria faults) that are responsible for the crustal seismicity occurring in this area. Morphological features of fault escarpments suggest long-term slip rates of 0.8–1.1 mm/year for the last 700 ky and values of 0.4–0.9 mm/year for the last 120 ky (Tortorici et al. 1995; Aloisi et al. 2013).

A few earthquakes of magnitude $M \geq 6.0$ hit this region in the last four centuries as reported in CPTI15 (Catalogo Parametrico dei Terremoti Italiani) (Rovida et al. 2015) (Table 1, partly reproducing Table 1 of Console et al. 2017). Among the strongest historical events, an earthquake sequence characterized by multiple mainshocks in February–March 1783 caused extensive destructions in southern Calabria. Later on, two other catastrophic earthquakes destroyed the Sant'Eufemia gulf and the Messina Straits areas in 1905 and 1908, respectively. Only a few other earthquakes are reported for the previous centuries, so that the application of statistical analysis to historical observations for a robust evaluation of the recurrence time of these earthquakes is unsuitable.

Although it is generally recognized that the major Calabria earthquakes were caused by normal faults rupturing the upper crust of the southern Calabria-Peloritani area (Boccaletti et al. 1984; Tortorici et al. 1995; Mattei et al. 1997; Serpelloni et al. 2010; D'Agostino et al. 2011; Presti et al. 2013), no consensus has been reached yet on seismogenic source location and orientation of these faults (Fig. 1). In particular, the source of the Messina 1908 earthquake is still strongly debated and several models of causative source have been put forward. Several authors hypothesized a blind low-angle normal fault dipping toward the SE and located below the Messina Straits (Capuano et al. 1988; Boschi et al. 1989; De Natale and Pingue 1991; Valensise and Pantosti 1992; Amoruso et al. 2002; Valensise et al. 2008; DISS Working Group 2015; De Natale and Pino 2014). Otherwise, NW dipping, high-angle normal faults on mainland Calabria have been proposed as causative sources of this earthquake (Schick 1977; Mulargia and Boschi 1983; Ghisetti 1984, 1992; Bottari et al. 1986; Westaway 1992; Tortorici et al. 1995; Bottari 2008; Aloisi et al. 2013, 2014; Minelli et al. 2016).

The DISS database includes, in the area considered in this study, also a group of NW-dipping sources (named A2-type faults by Tiberti et al. 2017) defined as Debated Seismogenic Sources because of the lack of quantitative information. Even if the inclusion of these antithetic faults in a unique seismogenic system would be an interesting exercise for the application of our earthquake simulator algorithm, at the present stage it remains a future task because the necessary geometric and kinematic information is not yet available.

The aeromagnetic survey in southern Calabria

Remotely sensed magnetic anomaly data provide an important means for helping delineate major crustal structures (e.g., Chiappini et al. 2002; De Ritis et al. 2007). Magnetic exploration is a potential field method that because of the nature of magnetic field and the magnetic characteristics of terrestrial materials, is widely used to determine location, shape and depths of the magnetic source, and it has been recently used in order to identify crustal scale features such as faults, dykes, intrusions (Blakely et al. 2002, 2014; Grauch et al. 2001; Nicolosi et al. 2006).

Consequently, the INGV Airborne Geophysics Team performed a high-resolution low-altitude aeromagnetic survey during September–October 2013. Geological interpretation and modeling (3-D inversion, forward modeling, and Euler deconvolution) of aeromagnetic data yielded three main tectonic features in southern Calabria (Minelli et al. 2016). The faults location partly matches the surface expression of already-known tectonic features (Cittanova, Serre and Armo faults, see Fig. 1). Moreover, magnetic data reveal an unknown Armo fault splay and the southward prosecution of the Cittanova fault through the Aspromonte massif. Such fault has been hypothesized to join toward the north with the Serre fault and then to represent a unique structure named Cittanova-Aspromonte-Serre fault (Fig. 2).

The parameters of the three seismogenic faults, recognized from the analysis of the aeromagnetic anomalies and used as input fault model for the simulation, are reported in Table 2, where latitude, longitude and depth refer to the upper left corner of the rectangular fault observed from the hanging wall, with the strike oriented to the right. Relying on field evidence (Galli and Bosi 2004; Aloisi et al. 2013), fault dip and rake were systematically set to 60° and 270° (respectively), while considering seismogenic layer thickness observed in Italy (ISIDE data base), fault width was assumed to be 17 km. Slip rates of the Armo and Cittanova-Aspromonte fault were set at 0.45 and 0.60 mm/year (respectively) after Aloisi et al. (2013) and Galli and Bosi (2004). Lacking literature data, the slip rate along the Armo fault splay has been equated to that of the Armo fault.

Algorithm of the simulator code

The algorithm of our simulator was initially introduced by Console et al. (2015) and successively modified by Console et al. (2017, 2018). This algorithm basically reflects the principle that the accumulated tectonic stress, or a known fraction of it, is released by co-seismic slip on a number of fault patches when they rupture during an earthquake.

We followed the approach adopted by Tullis (2012) for earthquakes simulators in California. No rheological constitutive laws (i.e., rate and state friction, pore fluid migration or viscosity) are introduced. The algorithm is mainly based on the theory of elasticity, including stress transfer among fault patches, and a couple of euristic rules determining the value of the tectonic stress necessary for initiating, expanding and terminating a rupture.

Initially, a randomly variable stress is arbitrarily assigned to each cell of the rectangular faults.

The tectonic loading is modeled by means of the slip rate adopted for every single fault. The conversion between slip and stress is computed through the relation suggested by Console and Catalli (2007) for a rectangular fault:

$$\sigma = \frac{32}{\pi^2}\mu\frac{s}{(WL)^{1/2}}, \quad (1)$$

where σ is the stress, s is the slip, μ is the shear modulus, and W and L are the width and the length of the fault.

A new rupture is nucleated once the stress on a fault patch exceeds a given arbitrary threshold. Neither the random initial stress nor the stress threshold is relevant for the final features of the output synthetic catalog, once a sufficiently long time is allowed to reach a self-organized steady state of the system, without being included in the output catalog.

As already mentioned in Introduction, the propagation and stopping of an initiated rupture are controlled in two ways:

(a) reducing the effective strength on the patches through a sort of weakening mechanism adjusted by a constant called strength-reduction coefficient (S-R; Console et al. 2017); this parameter has a meaning similar to the η free parameter in the Virtual Quake simulator developed for California (Schultz et al. 2017).
(b) discouraging the propagation of a rupture beyond very long lengths through a free parameter called aspect-ratio coefficient (A-R; Console et al. 2017); this parameter is relevant only if it is smaller than the ratio between the length and the width of the considered fault.

At every new rupture of a fault patch, its stress is dynamically reduced by a value determined by the size of the expanding rupture. The interaction with other fault patches is expressed by the Coulomb stress change computed through the seismic moment released by each

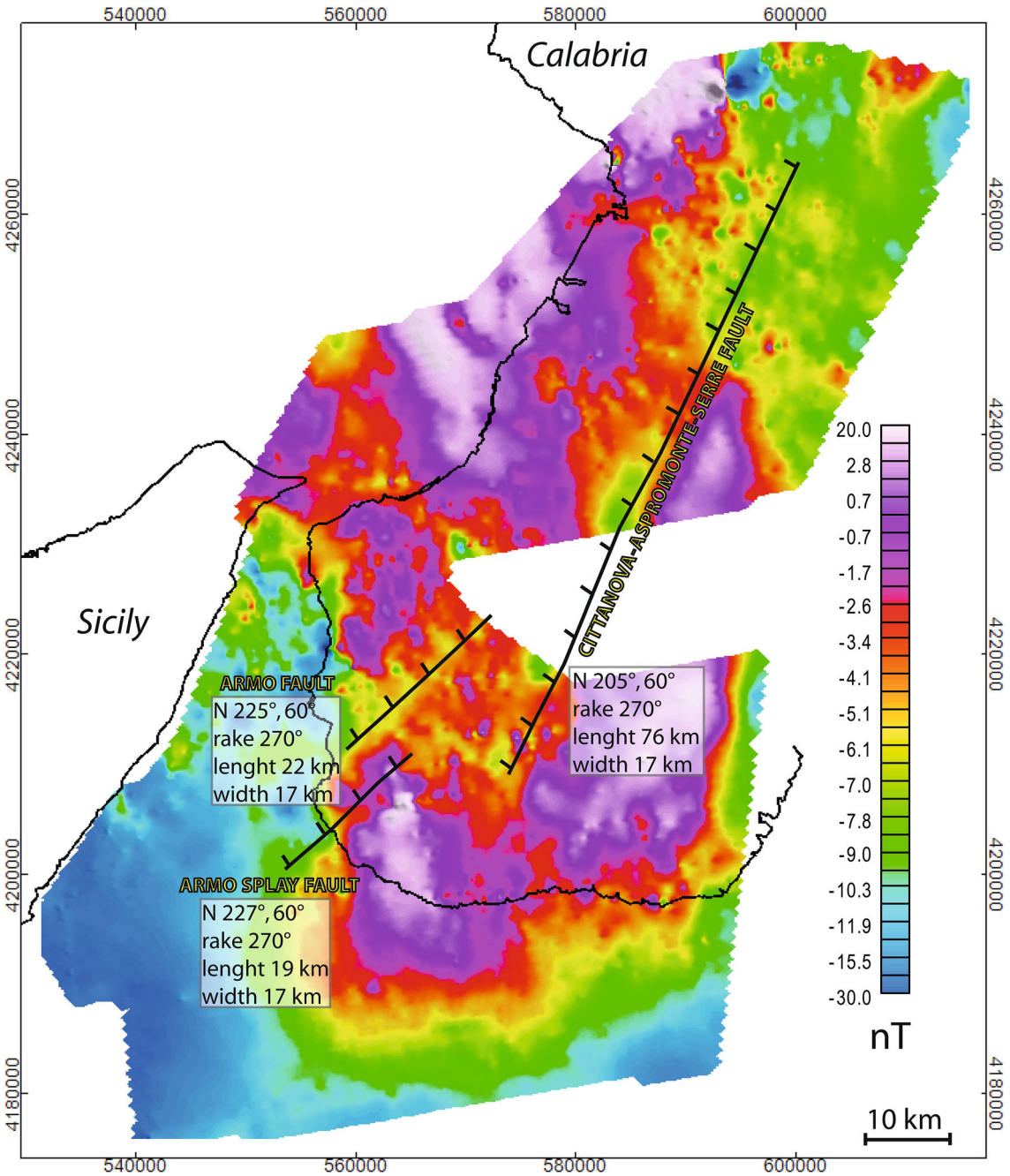

Fig. 2 Input fault model taken by high-resolution aeromagnetic anomaly data modeling and interpretation in southern Calabria. (e.g., Minelli et al. 2016). For each fault, the main fault parameters are detailed

Table 2 Source parameters of the southern Calabria fault system

Name	Latitude (°N)	Longitude (°E)	Depth (km)	Strike ϕ (°)	Dip δ (°)	Rake λ (°)	Length (km)	Width (km)	Slip Rate (mm/years)
Cittanova-Aspromonte-Serre	38.609	16.220	0.0	205	60	270	76	17	0.60
Armo	38.145	15.819	0.0	225	60	270	22	17	0.45
Armo Splay	38.004	15.715	0.0	227	60	270	19	17	0.45

ruptured patch, taking into account the source mechanism and the distance between each pair of patches.

When the rupture stops, the final value of the average slip, the source area, the seismic moment and the magnitude of the event are computed and stored in the output catalog. Recall that the magnitude distribution of the earthquakes in the synthetic catalog is not assigned. It is a consequence of the self-organized physical process of the simulator mode and can be changed by the choice of the free parameters S-R and A-R. As mentioned by Wilson et al. (2017), these simulation parameters are adjusted so that real earthquake catalogs are matched by synthetic catalogs in their scaling properties. For an analysis of the role of the S-R and A-R parameters in our simulation algorithm, see Console et al. (2017).

Application of the simulator to the southern Calabria region

In this study, we revisited the issue of seismic hazard assessment of the Calabria region, using basically the same methods introduced by Console et al. (2017), i.e., a simple attenuation law applied to a synthetic catalog obtained from the earthquake simulator. Here, we applied the same algorithms to a different database of seismogenic faults, obtained from the analysis of a recent aeromagnetic survey, limited to the southern part of the same region, as described in Sect. 3.

The three rectangular faults that represent the southern Calabria fault system (SCFS) reported in Table 2, according to recent seismotectonic interpretation of aeromagnetic data (Fig. 2), were discretized in patches of 0.5 km × 0.5 km. The minimum magnitude of an earthquake rupturing a single patch is approximately 3.4. The duration of the output catalog was 100 ky, not including a warm-up period of 20,000 years, sufficient to reach a standby status, independently of the initial stress random distribution of every patch.

In our simulation, an event generated by the simulator could have ruptured just a fraction of a single fault (moderate magnitude), or even an area larger than an entire fault (larger magnitudes), without any limit related to the size of the fault where the nucleation occurred.

On the basis of a series of tests carried out with different combinations of the free parameters, we chose the values of A-R = 10 and S-R = 0.6 in order to obtain a magnitude distribution with a *b*-value not far from 1.0 for the background seismicity with $M < 6.0$ (see also Console et al. 2017). In this application to southern Calabria, a particular care was devoted to the choice of the parameter A-R, which controls the largest magnitudes produced in the synthetic catalog, still maintaining the constraint of the total moment rate imposed by the tectonic slip rate assumed in the model. In our case, the Cittanova-Aspromonte-Serre fault, the largest of the three faults in the adopted model (Table 2), has an area of 76 km × 17 km = 1292 km^2. Minelli et al. (2016) remarked that an M ∼ 7.3 event would be expected from the entire rupture of this fault. In fact, according to two popular relationships between magnitude and rupture area (Wells and Coppersmith 1994, normal mechanism; WGCEP 2003, Ellsworth B, Eq. 4.5b), the rupture of the whole area of this fault would cause an earthquake of magnitude 7.29 and 7.31, respectively.

The application of the earthquake simulator to the SCFS produced a synthetic seismic catalog containing more than 18,000 $M \geq 4.0$ earthquakes. Figure 3 shows the epicentral map of a synthetic catalog of 5000 years along with the geometry of the input fault model. The time span of 5000 years is necessary to achieve a fairly even distribution of epicenters over the three faults. A shorter interval such as 1000 years would leave empty substantial portions of the faults areas.

Some numerical features of the synthetic catalog for earthquakes associated with single faults are reported in Table 3. Note that one event can be associated with more than one fault, when it has participated in substantial way to that event, as explained later in Sect. 5.2. The largest magnitudes for ruptures nucleating in each of the three

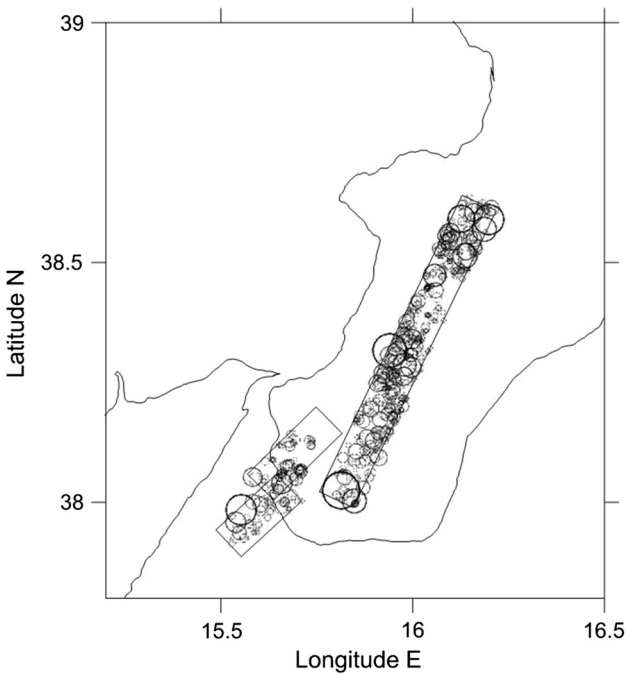

Fig. 3 Epicenter map of the synthetic earthquake catalog obtained with patches of 0.5 km × 0.5 km for the first 5000 years of simulation. The size of the black dots is scaled with magnitude from M4.0 to M6.6. The black rectangles denote the surface projection of the three faults of the input model

Table 3 Numerical features of the synthetic catalog produced by the simulator for single faults of the SCFS

Name	Number of events $M \geq 4.5$	Number of events $M \geq 6.0$	Largest magnitude
Cittanova-Aspromonte-Serre	2251	92	7.27
Armo	284	51	6.77
Armo Splay	293	50	6.76

faults, but not limited to only one of them, are 7.27, 6.77 and 6.76 for Cittanova-Aspromonte-Serre, Armo and Armo Splay, respectively.

Magnitude distribution

We show in Fig. 4 by blue diamonds the cumulative magnitude–frequency distribution of the 100,000 years catalog. It can be easily recognized that this plot is not fitted by a straight line as expected on the basis of the Gutenberg–Richter law. In fact, the magnitude distribution exhibits a different behavior in three separate magnitude ranges: a *b*-value equal to 1.23 in the $4.0 \leq M \leq 5.5$ range, a *b*-value equal to 0.60 in the $5.5 \leq M \leq 7.2$ range and a sharper decrease for $M \geq 7.3$. The scarcity of events of magnitude larger than 5.5 and the bump of the magnitude distribution around $7.0 \leq M \leq 7.2$ suggests that in some respect this range of magnitudes can be considered "characteristic" of the process modeled by our simulator. This feature is the result of the combination of the choices

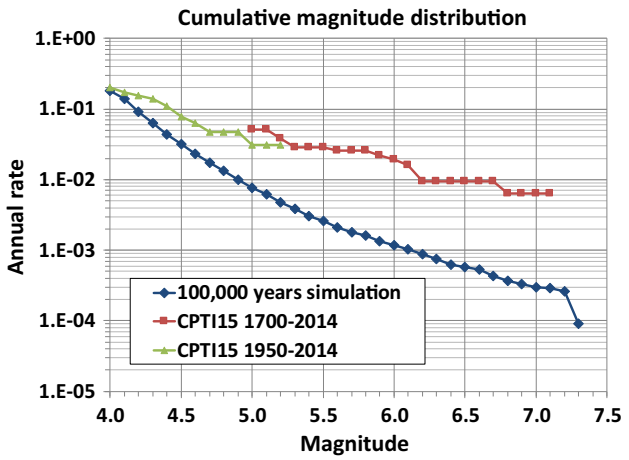

Fig. 4 Cumulative magnitude–frequency distribution of the synthetic catalog obtained from the simulation algorithm described in the text, compared with two real catalogs of earthquakes selected in the same areas. Blue diamonds: synthetic catalog lasting 100,000 years obtained using a discretization of 0.5 km × 0.5 km, an aspect-ratio (A-R) coefficient equal to 10 and a stress reduction (S-R) coefficient equal to 0.6. Red squares: CPTI15 catalog of the last 314 years and $M \geq 5.0$. Green triangles: catalog of the last 64 years and $M \geq 4.0$

for the free parameters S-R and A-R. However, this might also be a consequence of the characteristic dimensions of the sources adopted in the input geological model, the length of which is 76, 22 and 19 km, respectively. Earthquakes of magnitude larger than *M*6.8 can only be caused by the rupture of a large fraction of the longest fault or by the joint ruptures of more than one source in a unique event.

It is interesting to compare the magnitude–frequency plot of our synthetic catalog with similar distributions obtained from real observations. For this purpose, we have selected two data samples from the Historical Italian Catalog, CPTI15 (Rovida et al. 2015) in the study area of southern Calabria. The first data sample contains 17 earthquakes reported after 1700 A.D. for $M \geq 5.0$ (red squares in Fig. 4), and the second 13 earthquakes reported after 1950 A.D. for $M \geq 4.0$ (green triangles in Fig. 4). The magnitude–frequency distribution of the first sample is characterized by a *b*-value equal to 0.56 only, and that of the second sample by a b-value of 0.68. These low b-values could be caused by incompleteness of the catalog, as actually for the longest sample we chose a magnitude threshold of 5.0, which is smaller than the completeness magnitude of 5.8 estimated by the authors of CPTI15 for the time period after 1700 A.D. in Southern Italy. However, a similarly small *b*-value is shown also by a shorter sample of 8 $M \geq 5.0$ earthquakes starting in 1870.

We may also note that the annual rate of $M \geq 5.0$ earthquakes contained in the synthetic catalog is less than 1 per century, while the annual rate estimated from the historical catalog is at least five times larger. The higher rate of moderate magnitude earthquakes reported in the historical catalog could be ascribed to the existence of smaller sources that are not considered in the simplified model consisting only of large-size sources. In fact, for selecting the earthquakes from the CPTI15 catalog, we considered the whole southern Calabria geographical region, and not the smaller area covered by the surface projections of the three faults of the model.

The occurrence of two $M \geq 7.0$ earthquakes reported in the historical catalog after 1700 A.D. (1783 and 1908) would imply a seismic moment rate of the order of at least $3.6\ 10^{17}$ Nm, much larger than the total rate of $6.6\ 10^{16}$ Nm obtained from the physics-based simulator, even without taking into account a possible fraction of strain released by aseismic slip. This inconsistency could be explained in different ways, including overestimation of the size of old historical earthquakes, underestimation of the slip rates adopted for the geological fault model and also possible long-term variations of seismic moment rate, which would imply the necessity of a much longer period of observations in order to allow a robust statistical analysis. In similar way, Carafa et al. (2017), in a discussion on the

discrepancy between the seismic moment rate inferred from the earthquake catalog for the last 480 years and that obtained from a model based on the long-term horizontal velocities in southern Calabria, concluded that the past 480 years would be simply too short of an interval for determining reliable long-term seismicity rates.

Considering the magnitude–frequency distribution of the shortest sample (shown by green triangles in Fig. 4), the comparison with the synthetic catalog shows a substantial similarity of seismic rate at about $M4.0$, but this sample is too short to allow any information for $M \geq 5.2$.

In agreement with Wilson et al. (2017), we may conclude that the size and the quality of the historical seismicity observed in the study area are too limited for achieving a robust comparison with the simulations.

Analysis of the strong earthquakes in the synthetic catalog

The problem faced by a seismologist who wants to study the recurrence time of an earthquake that can be considered as "characteristic" for a specific fault is the definition of a characteristic event. We have seen that the simulation algorithm does not turn out only with earthquakes with characteristic magnitude of specific faults, but with a wide magnitude distribution including magnitudes associated with ruptures on sources larger than a single fault.

In order to carry out a statistical analysis on the number of ruptured SFSs contributing to a single earthquake and their recurrence intervals, some quantitative, even if somehow arbitrary, definitions are necessary to assign a specific earthquake to one or more SFSs. For a more in-depth analysis of this issue, we refer to the discussion made by Field (2015) addressing the "recurrence of what?" question. More recently, Parsons et al. (2018) have pointed out that for seismic hazard calculations, the appropriate way to count earthquakes is to consider their participation at points, or short zones along faults, because it is participation that will govern the rate of strong shaking rather than nucleation.

Proceeding with a merely empirical way, we define a "strong" earthquake in the following way:

1. the minimum magnitude for the entire rupture is 6.0;
2. the earthquake is initially assigned to the fault containing most of the ruptured cells;
3. if the number of cells ruptured by the earthquake in one of the other faults is larger than 150 or this fault has at least 50% of ruptured patches, we consider that fault section to have ruptured in that particular earthquake.

In this way, we could count the number of times that a given fault contributed to any $M \geq 6.0$ earthquake either alone or together with other faults in the synthetic catalog. The results are reported in Table 4. This table clearly shows that quite a substantial fraction (35%) of the largest earthquakes reported in the synthetic catalog did rupture more than one fault segment, a consequence of the fact that the borders of single fault segments do not represent a barrier to the propagation of rupture between two segments.

Table 4 Number of $M \geq 6.0$ synthetic earthquakes associated with a different number of faults during the same event

Number of ruptured faults per event	Number of events
1	69
2	9
3	28

We might be interested in testing whether the earthquakes generated by the simulator on single faults behave as a time-independent Poisson process or not. For this test, we performed a statistical analysis of the inter-event times of the synthetic catalog for single faults. Figure 5 displays for each of three faults considered in this study the recurrence time distribution of the characteristic events defined in the above-mentioned empirical way. The statistical parameters obtained by this procedure for each fault of the SCFS are reported in Table 5 in the following order: average recurrence time for $M \geq 6.0$, T_r; probability of rupturing in 50 yrs, P_{50}; standard deviation of the recurrence times, σ; coefficient of variation, C_v, equal to σ/T_r.

Figure 5 and Tables 4 and 5 show that the overall activity of the northern (Cittanova-Aspromonte-Serre) fault is higher than that of the other two faults, due to its larger dimensions and slip rate (Table 2).

The coefficient of variation C_v is 0.75 for the Cittanova-Aspromonte-Serre fault and close to 0.6 for the other two sources, which would denote a somewhat pseudo-periodicity of the earthquake occurrence. Let's here recall that a perfect periodicity is characterized by $C_v = 0$ and a time-independent Poisson process by $C_v = 1$. However, Fig. 5 denotes a bimodal behavior of the inter-event time distributions. In particular, the distribution obtained for the Cittanova-Aspromonte source exhibits two clear maxima: one for inter-event times smaller than 1200 years and the other for inter-event times between 2000 and 2500 years.

A comparison of the results obtained by our approach can be tried with a different approach used to define a characteristic model for each fault. For this comparison, we consider the information reported in the Database of Individual Seismic Sources maintained by INGV. It is relevant to mention that in this particular area of the Italian territory the individual sources are just a little smaller, but

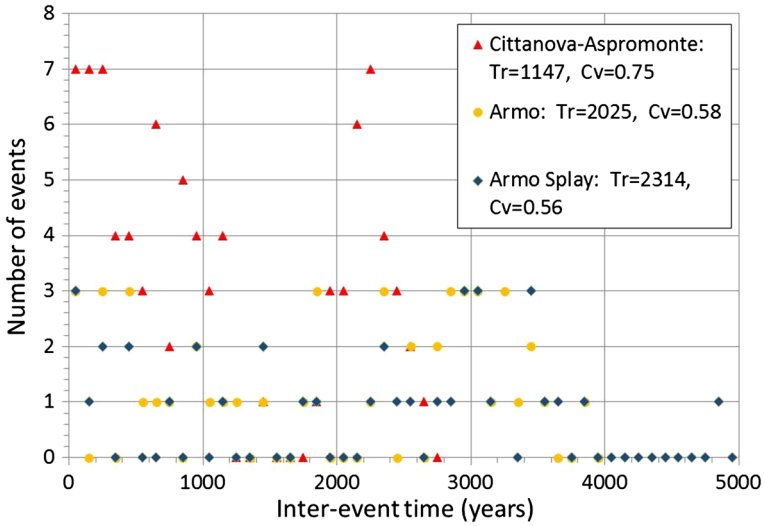

Fig. 5 Inter-event time distribution for $M \geq 6.0$ earthquakes from a simulation of 100 ky of seismic activity across the SCFS system for the three faults recognized in this study

Table 5 Results of the statistical analysis on the simulated seismicity for the SCFS

Source name	T_r ($M \geq 6.0$) (years)	P_{50} (%)	σ (years)	C_v
Cittanova-Aspromonte-Serre	1147	4.26	865	0.75
Armo	2025	2.44	1178	0.58
Armo Splay	2314	2.14	1286	0.56

Table 6 Parameters of the three individual faults reported in the DISS database for the southern Calabria region

Source name	Length (km)	Width (km)	Maximum magnitude	Slip rate (mm/years)	T_r (years)
Upper Mesima Basin	22.0	13.5	6.6	0.1–1.0	1090–10,900
Gioia Tauro Plain	25.0	15.0	6.6	0.1–1.0	860–8600
Messina Straits	40.0	20.0	7.0	0.93–2.0	710–1527

substantially overlapping the composite seismogenic sources (DISS Working Group 2015), which are considered suitable for a physical modeling of the seismogenic process.

As shown in Table 6, this database includes three individual faults recognized in the area of our study from North to South: Upper Mesima Basin, Gioia Tauro Plain and Messina Straits (see Fig. 1 for fault location). Very large uncertainties of a factor of ten affect the recurrence time Tr for the first two faults (Upper Mesima Basin and Gioia Tauro Plain). Unlike the model used in our simulator, in which the northernmost fault (Cittanova-Aspromonte) is the largest of the system, the DISS database lists the southernmost fault (Messina Straits) as the largest of the three. Moreover, there is a basic difference in modeling the seismic process, consisting in the fact that our simulation algorithm allows all the three sources to rupture in the same earthquake, while the DISS database considers only events rupturing a single fault.

Taking into account the differences of methodological kind, an overall comparison is still possible between the occurrence rates obtained by our and DISS approaches for earthquakes of magnitude $M \geq 6.6$. Our model (Fig. 4) shows a recurrence time of about 1820 years for such earthquakes. The combination of the occurrence rates for the three faults listed in Table 6, assumed as independent Poisson processes, gets a recurrence time ranging from 287 to 1160 years. In few words, our simulation produces an overall rate of $M \geq 6.6$ earthquakes substantially smaller than that inferred from the DISS database, even considering the smallest slip rate (or the largest recurrence times) reported in this database. Conversely, our approach allows much of the seismic moment rate to be released by stronger, but less frequent, earthquakes.

The simulated catalog applied to seismic hazard assessment

With the aim of exploring a potential application of the synthetic catalog obtained by the simulation algorithm to seismic hazard assessment, we followed a simple

procedure applying the Cornell (1968) method to the $M \geq 4.0$, 100 ky synthetic catalog.

We computed the PGA (Peak Ground Acceleration) at a dense grid of points covering the territory of the Calabria region for each earthquake of the catalog by means of a popular attenuation law (Sabetta and Pugliese 1987):

$$\log(PGA) = -1.562 + 0.306M - \log\left(\sqrt{d^2 + 5.8^2}\right) + 0.169S_1 + 0.169S_2 \pm 0.173, \quad (2)$$

where M is the earthquake magnitude, d is the epicentral distance, and S_1 and S_2 are parameters ranging from 0 to 1, accounting for the soil dynamic features at the receiving site, with a factor of more than 2 for PGA from hard rock to extremely soft soil. In lack of a detailed knowledge of the soil conditions in each site of the study region, we have adopted the choice $S_1 = 0$ and $S_2 = 1$, equivalent to $S_1 = 1$ and $S_2 = 0$. As the purpose of this section is only to give an example of the potential use of a synthetic catalog for seismic hazard assessment, we did not include an analysis of the uncertainties on the results.

At each node of the grid, we computed the number of times that a given PGA was exceeded in 100 ky, and from its distribution, the value of PGA characterized by the probability of exceedance of 10% in 50 years. The results shown in Fig. 6 provide an example of how the method works.

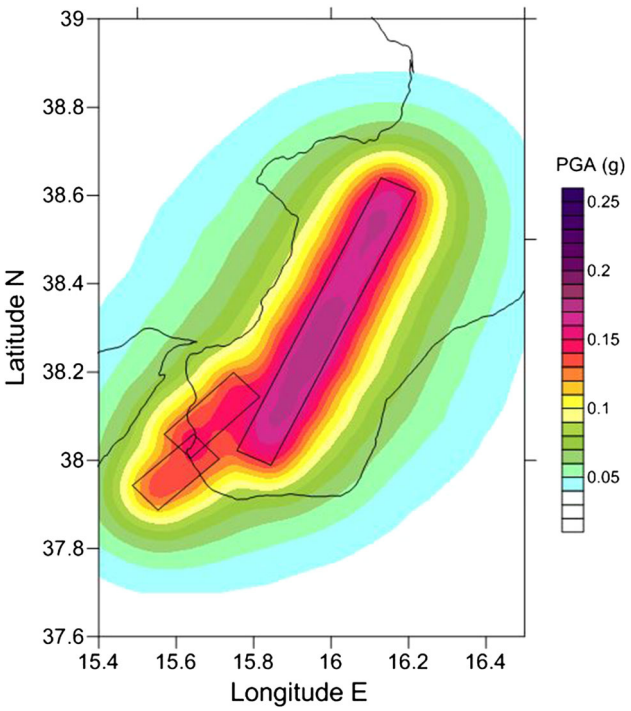

Fig. 6 PGA with 10% probability of exceedance in 50 years in Calabria region, obtained from the method described in the text. The black rectangles denote the geometric position of the three faults of the input model

We retained interesting to make a comparison of the results obtained in this section in terms of probability of PGA exceedance with those reported in previous studies.

We tried this comparison with the following sources:

(a) The national seismic hazard map issued on March 30, 2003 in annex to the Ordinance of the President of the Council of Ministers (and subsequently updated until 2015) (Fig. 7a);
(b) A previous study dealing with simulations based on the national seismic source catalog maintained by INGV (DISS Working Group 2015) (Fig. 7b).

The comparison of the contour levels supports a similarity of our results with the values given in the present Italian seismic building code, even though they are based on a different methodology. The fact that our values are about 30% lower than the 50th percentile of the Italian seismic building code (Fig. 7a) can be ascribed to our arbitrary choice of the values for the S_1 and S_2 parameters in Eq. (2). However, this difference is largely covered by the uncertainty of $\pm$ 0.173 in logarithmic scale (49% in linear scale) for the PGA in Eq. (2).

The same similarity cannot be recognized for the comparison of our present study with the results shown in Fig. 7b, obtained from a previous study based on our same methodology but with a different geological model (Console et al. 2017). In order to allow an easier comparison, we have converted the original scale (probability of exceeding a 0.2 g PGA in 50 years) into PGA values having a 10% probability of exceedance in 50 years. The much more scattered pattern of Fig. 7b is explained by the larger variability of the slip rate adopted for the single faults in the input geological model (Console et al. 2017), which is much smaller in southern Calabria, except for the Messina Straits fault.

Conclusions

In this study, we explored the potential utility of a multi-methodological approach to seismic hazard assessment, applying this approach to the study of the seismicity of the southern Calabria fault system. As input seismotectonic data, we used for the first time fault parameters gathered from a high-resolution aeromagnetic survey of southern Calabria (Minelli et al. 2016). Magnetic anomalies probe the entire upper crust geometry and characteristics, and thus they are more representative of seismogenic layer setting than surface geological surveys.

We can draw the following conclusions from the results of this study:

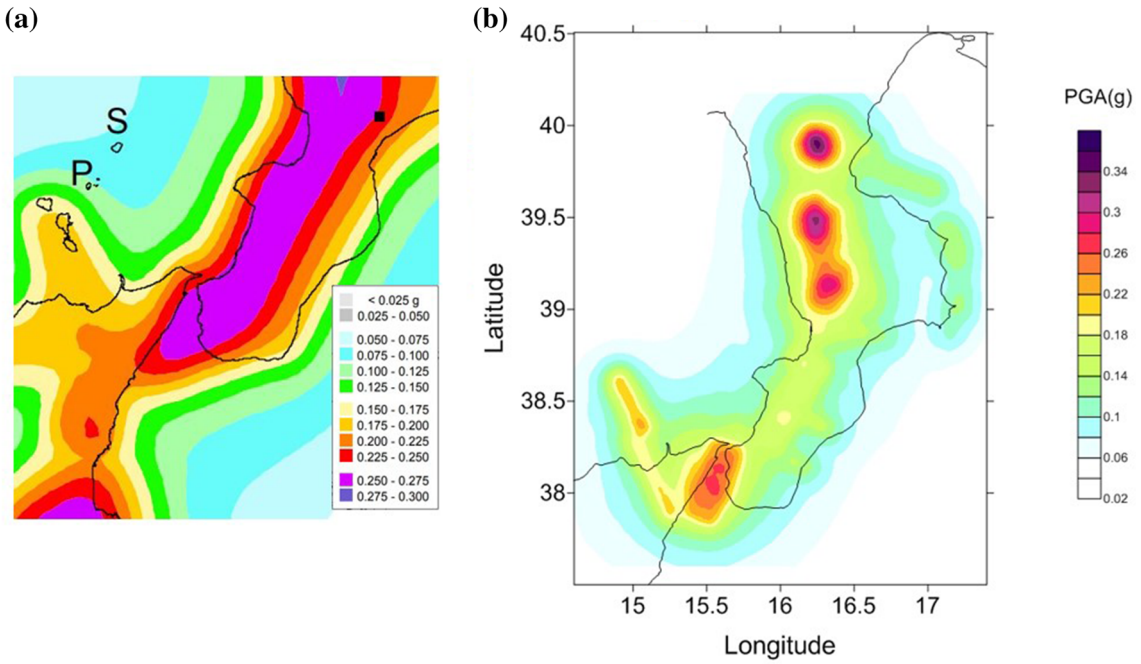

Fig. 7 Probabilistic seismic hazard assessments obtained by alternative methods with respect to this study: **a** the national seismic hazard map, showing the 50th percentile of the statistical distribution; **b** a previous study similar to the present one, but adopting the national seismic source catalog (DISS Working Group 2015) (Console et al. 2017). The color scale represents the PGA values with an exceedance probability of 10% in 50 years

1. The earthquake simulator algorithm adopted in this study is based on a relatively simple physical model that does not rely on detailed physical laws such as rate-state friction; in this respect, it can be regarded as an alternative to other physics-based earthquake simulators, providing interesting practical applications due to the low computational costs.
2. The application of the earthquake simulator has allowed the compilation of a long-term seismic catalog, which has a much longer duration than the catalog based on real historical information.
3. The frequency–magnitude distribution of the simulated seismicity is not fully consistent with a Gutenberg–Richter distribution and is characterized by different b-values in the ranges of small, moderate and large magnitudes.
4. The statistical distribution of inter-event times of earthquakes with $M \geq 6.0$ on single faults is consistent with a fairly pseudo-periodic behavior, with a coefficient of variation C_v close to 0.60–0.75.
5. The synthetic catalog obtained from the simulation can be easily used for seismic hazard assessment allowing the computation of the PGA threshold characterized by a given exceedance probability in a given time interval.
6. The map reporting the PGA values characterized by a 10% probability of exceedance in 50 years obtained in this study for the southern Calabria area is fairly well consistent with the seismic hazard map adopted by the present Italian seismic building code.
7. The most critical aspects in the uncertainties affecting the seismic hazard assessment obtainable by the methodologies introduced in this study can be recognized in the values of slip rates adopted for the faults of the seismotectonic model and the adopted PGA attenuation law.

This study was mainly aimed at exploring methodological aspects and potential capabilities of alternative observation techniques and simulation algorithms. However, the initial results obtained by our study encourage the application of these new approaches, jointly with other more extensively adopted methodologies for time-independent and time-dependent seismic hazard assessment.

Acknowledgements The authors are grateful to the Associate Editor, David Rhoades, and two anonymous reviewers for their useful comments and suggestions. On behalf of all the authors, the corresponding author states that there is no conflict of interest.

References

Aloisi M, Bruno V, Cannavò F, Ferranti L, Mattia M, Monaco C, Palano M (2013) Are the source models of the M 7.1 1908 Messina Straits earthquake reliable? Insights from a novel inversion and a sensitivity analysis of leveling data. Geophys J Int 192:1025–1041. https://doi.org/10.1093/gji/ggs062

Aloisi M, Bruno V, Cannavò F, Ferranti L, Mattia M, Monaco C (2014) Reply to 'Comments on the paper "Are the source models of the M 7.1 1908 Messina Straits earthquake reliable? Insights from a novel inversion and sensitivity analysis of levelling data" by Aloisi et al. (2012). Geophys J Int 197:1403–1409. https://doi.org/10.1093/gji/ggu116

Amoruso A, Crescentini L, Scarpa R (2002) Source parameters of the 1908 Messina Straits, Italy, earthquake from geodetic and seismic data. J Geophys Res 107(B4):2080. https://doi.org/10.1029/2001JB00043

Blakely RJ, Wells RE, Weaver CS, Johnson SY (2002) Location, structure, and seismicity of the Seattle fault zone, Washington: evidence from aeromagnetic anomalies, geologic mapping, and seismic-reflection data. GSA Bull 114(2):169–177

Blakely RJ, Sherrod BL, Weaver CS, Wells RE, Rohay AC (2014) The Wallula fault and tectonic framework of south-central Washington, as interpreted from magnetic and gravity anomalies. Tectonophysics 624–625:32–45

Boccaletti M, Nicolich R, Tortorici L (1984) The Calabrian Arc and the Ionian Sea in the dynamic evolution of the central Mediterranean. Mar Geol 55:219–245

Boschi E, Pantosti D, Valensise G (1989) Modello di sorgente per il terremoto di Messina del 1908 ed evoluzione recente dell'area dello Stretto, in *Atti VIII Convegno G.N.G.T.S.*, Roma, pp 245–258

Bottari A (2008) Osservazioni macrosismiche e studi, in Riassunti estesi del Convegno 1908–2008 Scienza e Società a cento anni dal Grande Terremoto, Reggio Calabria 10–12 dicembre 2008, Miscellanea I.N.G.V., 3, 19–20

Bottari A, Carapezza E, Carapezza M, Carveni P, Cefali F, Lo Giudice E, Pandolfo C (1986) The 1908 Messina Strait earthquake in the regional geostructural frame work. J Geodyn 5:275–302

Capuano P, De Natale G, Gasparini P, Pingue F, Scarpa R (1988) A model for the 1908 Messina Straits (Italy) earthquake by inversion of leveling data. Bull Seism Soc Am 78:1930–1947

Carafa MMC, Kastelic V, Bird P, Maesano FE, Valensise G (2017) A "Geodetic Gap" in the Calabrian Arc: evidence for a locked subduction Megathrust?. Res Lett, Geoph. https://doi.org/10.1002/2017GL076554

Chiappini M, Ferraccioli F, Bozzo E, Damaske D (2002) Regional compilation and analysis of aeromagnetic anomalies for the Transantarctic Mountains-Ross Sea sector of the Antarctic. Tectonophysics 347:121–137

Christophersen A, Rhoades DA, Colella HV (2017) Precursory seismicity in regions of low strain rate: insights from a physics-based earthquake simulator. Geophys J Int 2017(209):1513–1525. https://doi.org/10.1093/gji/ggx104

Console R, Catalli F (2007) A rate-state model for aftershocks triggered by dislocation on a rectangular fault: a review and new insights. Ann Geophys 49(6):1259–1273

Console R, Carluccio R, Papadimitriou E, Karakostas V (2015) Synthetic earthquake catalogs simulating seismic activity in the Corinth Gulf, Greece, fault system. J Geophys Res 120(1):326–343. https://doi.org/10.1002/2014JB011765

Console R, Nardi A, Carluccio R, Murru M, Falcone G, Parsons T (2017) A physics-based earthquake simulator and its application to seismic hazard assessment in Calabria (Southern Italy) region. Acta Geophys 65(1):243–257. https://doi.org/10.1007/s11600-017-0020-2

Console R, Vannoli P, Carluccio R (2018) The seismicity of the Central Apennines (Italy) studied by means of a physics-based earthquake simulator. Geophys J Int 212:916–929. https://doi.org/10.1093/gji/ggx451

Cornell CA (1968) Engineering seismic risk analysis. Bull Seism Soc Am 58:1583–1606

D'Agostino N, D'Anastasio E, Gervasi A, Guerra I, Nedimović Mladem R, Seeber L, Steckler M (2011) Forearc extension and slow rollback of the calabrian arc from GPS measurements. Geophys Res Lett 38:L17304. https://doi.org/10.1029/2011GL048270

De Natale G, Pingue F (1991) A variable slip fault model for the 1908 Messina Straits (Italy) earthquake, by inversion of leveling data. Geophys J Int 104:73–84

De Natale G, Pino NA (2014) Comment on 'Are the source models of the M 7.1 1908 Messina Straits earthquake reliable? Insights from a novel inversion and sensitivity analysis of levelling data' by M. Aloisi, V. Bruno, F. Cannavò, L. Ferranti, M. Mattia, C. Monaco and M. Palano. Geophys J Int 197:1399–1402. https://doi.org/10.1093/gji/ggu063

De Ritis R, Ventura G, Chiappini M (2007) Aeromagnetic anomalies reveal hidden tectonic and volcanic structures in the central sector of the Aeolian Islands, Southern Tyrrhenian Sea, Italy. J Geophys Res 112:B10105. https://doi.org/10.1029/2006JB004639

DISS Working Group (2015). Database of Individual Seismogenic Sources (DISS), Version 3.2.0: a compilation of potential sources for earthquakes larger than M 5.5 in Italy and surrounding areas. http://diss.rm.ingv.it/diss/, Istituto Nazionale di Geofisica e Vulcanologia; https://doi.org/10.6092/ingv.it-diss3.2.0

Field EH (2015) Computing elastic-rebound-motivated earthquake probabilities in unsegmented fault models: a new methodology supported by physics-based simulators. Bull Seism Soc Am 105(2A):544–559. https://doi.org/10.1785/0120140094

Galli P, Bosi V (2004) Catastrophic 1638 earthquakes in Calabria (southern Italy): new insights from paleoseismological investigation. J Geophys Res 108(B1):2003. https://doi.org/10.1029/2001JB001713

Ghisetti F (1984) Recent deformations and the seismogenic source in the Messina Straits (southern Italy). Tectonophysics 109:191–208

Ghisetti F (1992) Fault parameters in the Messina Straits (southern Italy) and relations with the seismogenic source. Tectonophysics 210:117–133

Grauch VJS, Hudson MR, Minor SA (2001) Aeromagnetic expression of faults that offset basin fill, Albuquerque basin, New Mexico. Geophysics 66(3):707–720

Hanks TC, Kanamori HD (1979) A moment magnitude scale. J Geophys Res 84(B5):2348–2350

Mattei M, Sagnotti L, Faccenna C, Funiciello R (1997) Magnetic fabric of weakly deformed clay-rich sediments in the Italian peninsula: relationships with compressional and extensional tectonics. Tectonophysics 271:107–122

Minelli L, Vecchio A, Speranza F, Nicolosi I, D'Ajello Caracciolo F, Chiappini S, Carluccio R, Chiappini M (2016) Aeromagnetic investigation of Southern Calabria and the Messina Straits (Italy): tracking seismogenic sources of 1783 and 1908 earthquakes. J Geophys Res Solid Earth 121. https://doi.org/10.1002/2015jb012305

Mulargia F, Boschi E (1983) The 1908 Messina earthquake and related seismicity, in earthquakes: observation, theory and interpretation. In: Kanamori H, Boschi E (eds) Proceedings of the international school of physics Enrico Fermi, course, vol 85. Elsevier, Amsterdam, pp 493–518

Nicolosi I, Blanco-Montenegro I, Pignatelli A, Chiappini M (2006) Estimating the magnetization direction of crustal structures by means of an equivalent source algorithm. Phys Earth Planet Interiors. https://doi.org/10.1016/j.pepi.2005.12.003

Parsons T, Geist EL, Console R, Carluccio R (2018) Earthquake magnitude frequency on California faults calculated from consensus data. J Geoph Res (**submitted**)

Presti D, Billi A, Orecchio B, Totaro C, Faccenna C, Neri G (2013) Earthquake focal mechanisms, seismogenic stress and seismotectonics of the Calabrian Arc, Italy. Tectonophysics 602:153–175

Rovida A, Camassi R, Gasperini P, Stucchi M (eds) (2015) CPTI15, the 2015 version of the Parametric Catalogue of Italian Earthquakes. INGV, Milano, Bologna. http://doi.org/10.6092/INGV.IT-CPTI15 (http://emidius.mi.ingv.it/CPTI15)

Sabetta F, Pugliese A (1987) Attenuation of peak horizontal acceleration and velocity from Italian strong motion records. Bull Seism Soc Am 77:1491–1513

Schick R (1977) Eine seismotektonische Bearbeitung des Erdbebens von Messina im Jahre 1908. Geologisches Jahrbuch, Reihe E 11, 74 pp

Schultz KW, Yoder MR, Wilson JM, Heien EM, Sachs MK, Rundle JB, Turcotte DL (2017) Parametrizing physics-based earthquake simulations. Pure Appl Geophys 174:2269–2278. https://doi.org/10.1007/s00024-016-1428-3

Serpelloni E, Bürgmann R, Anzidei M, Baldi P, Mastrolembo Ventura B, Boschi E (2010) Strain accumulation across the Messina Straits and kinematics of Sicily and Calabria from GPS data and dislocation modeling. Earth Plan Sci Lett 298:347–360. https://doi.org/10.1016/j.epsl.2010.08.005

Tiberti MM, Vannoli P, Fracassi U, Burrato P, Kastelic V, Valensise G (2017) Understanding seismogenic processes in the Southern Calabrian Arc: a geodynamic perspective, Italy. J Geosci 136(3):365–388. https://doi.org/10.3301/IJG.2016.12

Tortorici L, Monaco C, Tansi C, Cocina O (1995) Recent and active tectonics in the Calabrian Arc (Southern Italy). Tectonophysics 243:37–55

Tullis TE (2012) Preface to the focused issue on earthquake simulators. Seism Res Lett 83(6):957–958

Valensise G, Pantosti D (1992) A 125-Kyr-long geological record of seismic source repeatability: the Messina Straits (southern Italy) and the 1908 earthquake (MS 7 1/2). Terra Nova 4:472–483

Valensise G, Basili R, Burrato P (2008) La sorgente del terremoto del 1908 nel quadro sismotettonico dello Stretto di Messina. In: Bertolaso G et al (eds) Terremoto di Messina del 1908. Sorgente sismogenetica. Dipartimento Protezione Civile, Istituto Nazionale di Geofisica e Vulcanologia, Roma, pp 161–182

Wells DL, Coppersmith KJ (1994) New empirical relationships among magnitude, rupture length, rupture width, rupture area, and surface displacement. Bull Seism Soc Am 84(4):974–1002

Westaway R (1992) Seismic moment summation for historical earthquakes in Italy: tectonic implications. J Geophys Res 97(B11):15437–15464. https://doi.org/10.1029/92JB00946

Wilson JM, Yoder MR, Rundle JB, Turcotte DL, Schultz KW (2017) Spatial evaluation and verification of earthquake simulators. Pure appl Geophys 174:2279–2293. https://doi.org/10.1007/s00024-016-1385-x

WGCEP, Working Group on California Earthquake Probabilities (2003) Earthquake probabilities in the San Francisco Bay Region 2002–2031: U.S. Geological Survey Open-File Report 2003–2014. http://pubs.usgs.gov/of/2003/of03-214/

Yoder MR, Schultz KW, Heien EM, Rundle JB, Turcotte DL, Parker JW, Donnellan A (2015) The virtual quake earthquake simulator: a simulation-based forecast of the ElMayor-Cucapah region and evidence of predictability in simulated earthquake sequences. Geophys J Int 203:1587–1604. https://doi.org/10.1093/gji/ggv320